MNRAS **000**, 1–10 (2017) Preprint 18 October 2017 Compiled using MNRAS LATEX style file v3.0

A new all-sky map of Galactic high-velocity clouds from the 21-cm HI4PI survey

Tobias Westmeier[1]★
[1]*International Centre for Radio Astronomy Research (ICRAR), The University of Western Australia, 35 Stirling Highway, Crawley WA 6009, Australia*

Accepted XXX. Received YYY; in original form ZZZ

ABSTRACT

High-velocity clouds (HVCs) are neutral or ionised gas clouds in the vicinity of the Milky Way that are characterised by high radial velocities inconsistent with participation in the regular rotation of the Galactic disc. Previous attempts to create a homogeneous all-sky H I map of HVCs have been hampered by a combination of poor angular resolution, limited surface brightness sensitivity and suboptimal sampling. Here, a new and improved H I map of Galactic HVCs based on the all-sky HI4PI survey is presented. The new map is fully sampled and provides significantly better angular resolution (16.2 versus 36 arcmin) and column density sensitivity (2.3 versus 3.7×10^{18} cm^{-2} at the native resolution) than the previously available LAB survey. The new HVC map resolves many of the major HVC complexes in the sky into an intricate network of narrow H I filaments and clumps that were not previously resolved by the LAB survey. The resulting sky coverage fraction of high-velocity H I emission above a column density level of 2×10^{18} cm^{-2} is approximately 15 per cent, which reduces to about 13 per cent when the Magellanic Clouds and other non-HVC emission are removed. The differential sky coverage fraction as a function of column density obeys a truncated power law with an exponent of −0.93 and a turnover point at about 5×10^{19} cm^{-2}. H I column density and velocity maps of the HVC sky are made publicly available as FITS images for scientific use by the community.

Key words: ISM: clouds – Galaxy: halo – Galaxy: kinematics and dynamics – radio lines: ISM

1 INTRODUCTION

High-velocity clouds (HVCs) are gas clouds detected in the optical and ultraviolet, but most notably in the 21-cm line of neutral hydrogen, across much of the sky at radial velocities that are incompatible with the regular rotation of the Galactic disc. There is no general consensus on how to separate HVCs from gas at low and intermediate velocities. In the past, most authors applied a fixed velocity threshold of 90 or 100 km s^{-1} in the Local Standard of Rest (LSR). However, this is clearly insufficient, as Galactic disc emission still occupies such extreme velocities in some parts of the sky. An improved definition was proposed by Wakker (1991) who introduced a so-called *deviation velocity* of $v_{\rm dev}$ = 50 km s^{-1} to characterise HVCs as deviating by a fixed velocity separation from the maximally permissible velocity of Galactic disc emission in a given direction. Today, the concept of deviation velocity is the most commonly applied criterion for defining high-velocity gas, although the actual value of $v_{\rm dev}$ may differ from the one applied by Wakker (1991).

HVCs come in a wide range of sizes and shapes ranging from large complexes and streams, such as the Magellanic Stream (Mathewson et al. 1974) or complex C (Hulsbosch 1968), to (ultra-)compact and isolated HVCs (CHVCs/UCHVCs; Braun & Burton 1999; Adams et al. 2013). The discovery of 21-cm H I emission from HVCs by Muller et al. (1963) sparked an intense scientific debate about their spatial distribution and origin (e.g., Oort 1966). This debate was settled only recently when distance brackets or upper limits for several HVCs became available, most notably halo gas in the direction of the Large Magellanic Cloud (Savage & de Boer 1981), complex M (Danly et al. 1993), complex A (Wakker et al. 1996; van Woerden et al. 1999), complex C (Wakker et al. 2007; Thom et al. 2008), the Cohen Stream (Wakker et al. 2008), complex GCP (Wakker et al. 2008) and complex WD (Peek et al. 2016), confirming that HVCs are generally located several kpc above the Galactic plane in close proximity to the Milky Way. This rules out the hypothesis that HVCs are pri-

★ E-mail: tobias.westmeier@uwa.edu.au

mordial dark-matter haloes distributed throughout the Local Group (Blitz et al. 1999), instead suggesting diverse gas infall or outflow mechanisms as the origin of most of the clouds (Cox 1972; Bregman 1980; de Boer 2004; Lehner & Howk 2010; Fraternali et al. 2015; Fox et al. 2016; Marasco & Fraternali 2017). HVCs also contain significant components of ionised gas that can be traced with the help of optical and ultra-violet absorption spectroscopy (Sembach et al. 2003; Fox et al. 2006). For a comprehensive review of the properties and origin of HVCs the reader is referred to Wakker & van Woerden (1997), Wakker (2001) and van Woerden et al. (2004).

The issue of creating complete all-sky maps of HVCs has been strongly tied to the availability of homogeneous, sensitive, all-sky surveys of Galactic H I emission. An initial, rather patchy all-sky map of HVCs based on the combination of different data sources was presented by Bajaja et al. (1985). The map included data from the IAR 30-m antenna and already showed the general outline of several of the large HVC complexes known today, including the Magellanic Stream and Leading Arm, complex C and the anti-centre complex. A much improved HVC survey of the northern sky with the 25-m Dwingeloo radio telescope was presented by Hulsbosch & Wakker (1988). Their map reveals all of the large HVC complexes in the northern sky, including complexes A, C and M as well as the entire anti-centre complex. Wakker (1991) then combined the southern-hemisphere data from Bajaja et al. (1985) with the improved northern-hemisphere data from Hulsbosch & Wakker (1988) to create an all-sky HVC map which revealed for the first time the structure and kinematics of high-velocity gas across the entire sky, albeit at a fairly low angular resolution (also see Wakker & van Woerden 1997).

The possibilities of imaging HVCs across the entire sky were significantly improved by the new generation of sensitive H I surveys carried out towards the end of the 20$^{\rm th}$ century, particularly the Leiden/Dwingeloo Survey (LDS; Hartmann & Burton 1997), the IAR 30-m survey of the southern sky (Arnal et al. 2000; Morras et al. 2000) and the H I Parkes All-Sky Survey (HIPASS; Barnes et al. 2001). Despite being an extragalactic survey, HIPASS was successfully employed by Putman et al. (2002) to create an improved catalogue of HVCs in the southern hemisphere at much better angular resolution of 15.5 arcmin, but poor velocity resolution of 26.4 km s^{-1}. Similarly, de Heij et al. (2002a) extracted a catalogue of CHVCs from the LDS data. Both catalogues were merged by de Heij et al. (2002b) into an all-sky catalogue of CHVCs.

The LDS and IAR surveys were combined into the all-sky Leiden/Argentine/Bonn survey (LAB; Kalberla et al. 2005) which, in turn, was used by Westmeier (2007) to create a homogeneous all-sky map of HVCs at an angular resolution of about 36 arcmin. While this map covers the full sky at the same resolution and sensitivity for the first time, the poor angular resolution of the data does not sufficiently resolve the most compact HVCs as well as the small-scale structure within larger HVC complexes.

The purpose of this paper is to present an improved, homogeneous all-sky map of HVCs based on the new HI4PI all-sky (4π sr) H I survey (HI4PI Collaboration 2016). The HI4PI survey combines data from the Effelsberg–Bonn H I Survey (EBHIS; Kerp et al. 2011) in the northern hemisphere and the Galactic All-Sky Survey (GASS; McClure-Griffiths et al. 2009) in the southern hemisphere to create an all-sky survey of Galactic H I emission at a significantly better angular resolution of 16.2 arcmin. This results in a factor of 2.2 improvement in resolution – or a factor of about 5 in beam solid angle – compared to the previously available HVC map by Westmeier (2007) based on the LAB survey. The resulting HVC map reveals details on much smaller angular and physical scales than before. Selected data products from the new map have been made publicly available, and their use and scientific exploitation by the community are encouraged.

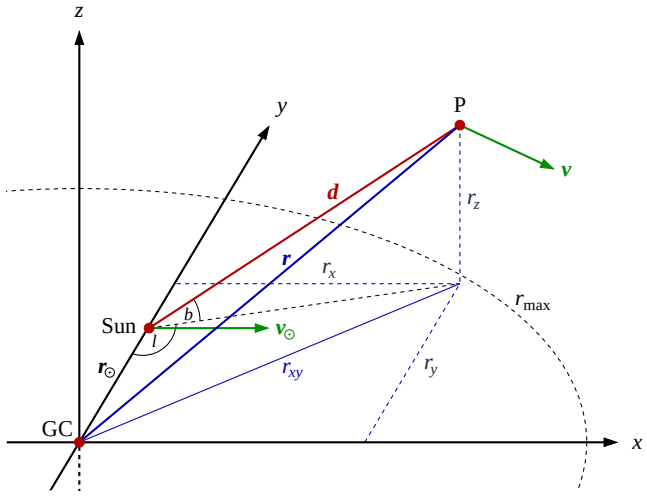

Figure 1. Illustration of the three-dimensional coordinate system and geometry assumed in the model of the Galactic disc, where an arbitrary point P with Galactic coordinates (l, b) is seen from the position of the Sun along the line-of-sight vector $\boldsymbol{d}$. GC denotes the Galactic centre.

This paper is organised as follows. In Section 2 the basic properties of the HI4PI survey are briefly described. Section 3 explains the masking of Galactic H I emission and the generation of HVC maps based on a simple model of the Milky Way. Section 4 discusses the resulting all-sky HVC map, including a comparison with the previous map from Westmeier (2007) based on the LAB survey. Lastly, the publicly released data products are introduced in Section 5 followed by a brief summary in Section 6.

2 THE HI4PI SURVEY

The HI4PI survey (HI4PI Collaboration 2016) combines H I data of the northern hemisphere from EBHIS (Kerp et al. 2011; Winkel et al. 2016) obtained with the 100-m Effelsberg radio telescope with comparable data of the southern hemisphere from GASS (McClure-Griffiths et al. 2009; Kalberla et al. 2010; Kalberla & Haud 2015) taken with the 64-m Parkes radio telescope. The GASS data were spectrally smoothed to the velocity resolution of EBHIS ($\Delta v \approx 1.5$ km s^{-1}) while the EBHIS data were smoothed to the angular resolution of GASS ($\vartheta \approx 16.2$ arcmin) to form a homogeneous all-sky survey of Galactic H I emission with a sensitivity of $\sigma_{\rm RMS} \approx 43$ mK. The latter corresponds to a $5\,\sigma_{\rm RMS}$ column density sensitivity of $N_{\rm H\,I} \approx 2.3 \times 10^{18}$ cm^{-2}, integrated over 20 km s^{-1}, for emission filling the beam. The

LSR velocity coverage is about ±480 km s^{-1} in the southern hemisphere and ±600 km s^{-1} in the northern hemisphere. The HVC map presented here is restricted to the narrower velocity coverage of the GASS data to ensure a homogeneous coverage across the sky. As virtually all HVC emission is restricted to velocities of $|v_{\rm LSR}| < 450$ km s^{-1}, the chosen velocity cut-off is not expected to have any effect on the quality and completeness of the HVC map.

3 DATA PROCESSING

3.1 Model of the Galactic H I disc

Creation of an all-sky HVC map requires masking of H I emission from the Galactic disc. Hence, the first step will be to develop a three-dimensional model of the Milky Way's neutral gas disc. For the sake of simplicity, a simple cylindrical geometry of the Galactic disc is assumed, similar to the approach by Wakker (1991) who concluded that the purity of the resulting HVC map is not particularly sensitive to the details of the model. The basic Galactocentric coordinate system used here is illustrated in Fig. 1, where the x and y axes define the Galactic plane, while the z axis is perpendicular to the plane and pointing in the direction of the north Galactic pole. The Sun is assumed to be located in the Galactic plane at the position of $\boldsymbol{r}_\odot = (0, r_\odot, 0)$ and moving in positive x-direction at a velocity of $\boldsymbol{v}_\odot = (v_\odot, 0, 0)$.[1] Throughout this paper the standard values of $r_\odot = 8.5$ kpc and $v_\odot = 220$ km s^{-1} adopted by the International Astronomical Union (Kerr & Lynden-Bell 1986) are assumed.

Let us further introduce a point P with radius vector $\boldsymbol{r} = (r_x, r_y, r_z)$ at which the gas is moving at a velocity of $\boldsymbol{v} = (v_x, v_y, 0)$. Following the geometry in Fig. 1, the position of P is given as

$$\boldsymbol{r} = \begin{pmatrix} r_x \\ r_y \\ r_z \end{pmatrix} = \begin{pmatrix} d\sin(l)\cos(b) \\ r_\odot - d\cos(l)\cos(b) \\ d\sin(b) \end{pmatrix} \quad (1)$$

where l and b are the Galactic longitude and latitude, respectively, of the line-of-sight vector, $\boldsymbol{d}$, pointing from the Sun to point P. Next, we need to determine the radial velocity of the gas at P relative to the Sun by projecting the velocity vector, $\boldsymbol{v}$, on to the line-of-sight vector, $\boldsymbol{d}$, and subtracting the projected contribution from the Sun's own orbital velocity, thus

$$v_{\rm rad} = \frac{\boldsymbol{d} \cdot (\boldsymbol{v} - \boldsymbol{v}_\odot)}{|\boldsymbol{d}|} = \frac{(\boldsymbol{r} - \boldsymbol{r}_\odot) \cdot (\boldsymbol{v} - \boldsymbol{v}_\odot)}{d}. \quad (2)$$

Inserting Eq. 1 into Eq. 2, we obtain the following expression for the radial velocity:

$$v_{\rm rad} = \left[v_{\rm rot}(r_{xy}) \frac{r_\odot}{r_{xy}} - v_\odot \right] \sin(l)\cos(b) \quad (3)$$

where $v_{\rm rot}(r_{xy})$ is the rotation curve of the Milky Way and $r_{xy} = |(r_x, r_y)|$. Note that the geometry used here implies cylindrical rotation, i.e. the rotation velocity of the disc is assumed to be independent of height, z, above the Galactic plane.

[1] Strictly speaking, this velocity refers to the LSR, as the Sun possesses a small peculiar motion with respect to the LSR.

For this work, the rotation curve of Clemens (1985) is used, specifically the polynomial fit to the rotation curve for the IAU standard values of $r_\odot = 8.5$ kpc and $v_\odot = 220$ km s^{-1}. The rotation curve of Clemens (1985) was derived from combined CO and H I observations of the Milky Way and should therefore be well-suited to describe the rotation velocity of the neutral gas disc for the purpose of identifying high-velocity emission.

With the radial velocity of any arbitrary point at hand, we can now determine the velocity range of Galactic disc gas for any position in the sky by simply moving away from the Sun in discrete steps along the line of sight, determining the radial velocity of the gas in each step, and recording the maximum and minimum values, $v_{\rm max}$ and $v_{\rm min}$, encountered in between the Sun and the boundary of the cylindrical disc model. Lastly, the derived velocity range will need to be expanded by a fixed deviation velocity, $v_{\rm dev}$, to account for the intrinsic velocity dispersion of the disc gas as well as any small deviations from the regular rotation velocity of the disc (Wakker 1991). The final velocity range, $[v_{\rm min} - v_{\rm dev}, v_{\rm max} + v_{\rm dev}]$, can then be masked in the data cube, leaving only channels with velocities inconsistent with Galactic rotation.

3.2 Optimisation of model parameters

While we now have a simple model of the Galactic disc that will allow us to mask and remove Galactic H I emission, there are several free parameters, specifically the disc size, $r_{\rm max}$ and $z_{\rm max}$, as well as the value of the deviation velocity, $v_{\rm dev}$, that will need to be chosen first. For this purpose, a low-resolution copy of the entire HI4PI survey was created by binning the data by a factor of 8 in the spatial domain and 4 in the spectral domain. This reduced the total data volume by a factor of 256, allowing for fast processing of the full sky at low resolution.

Next, maps of HVC emission were calculated from the binned data using a matrix of different values for the three free parameters. The following set of parameter values were tested in this way: $r_{\rm max} = 20$, 25 and 30 kpc, $z_{\rm max} = 2$, 5 and 10 kpc, and $v_{\rm dev} = 50$, 60 and 70 km s^{-1}. This resulted in a total of 27 different parameter combinations to be processed and tested. The HVC maps resulting from the different combinations of parameters were finally inspected by eye to determine the parameter values that would successfully remove most of the Galactic foreground H I emission while retaining as much of the H I emission from the HVC population as possible.

The resulting optimal set of disc parameters is $r_{\rm max} = 20$ kpc, $z_{\rm max} = 5$ kpc and $v_{\rm dev} = 70$ km s^{-1}. Interestingly, varying the value of $r_{\rm max}$ did not have any significant influence on the result, while changing the thickness of the disc led to substantial changes in the purity of the resulting HVC map. Similarly, choosing a lower deviation velocity would introduce significant residuals from intermediate-velocity gas, e.g. in the region of complex M. Compared to the parameters adopted by Wakker (1991), the disc radius chosen here is smaller, while the thickness of the disc and deviation velocity are larger. This results in a 'cleaner' map with lower levels of residual emission from the Galactic disc (e.g. in the region of the Outer Arm), while the major HVC complexes are largely unaffected due to their significant kinematic separation from the disc.

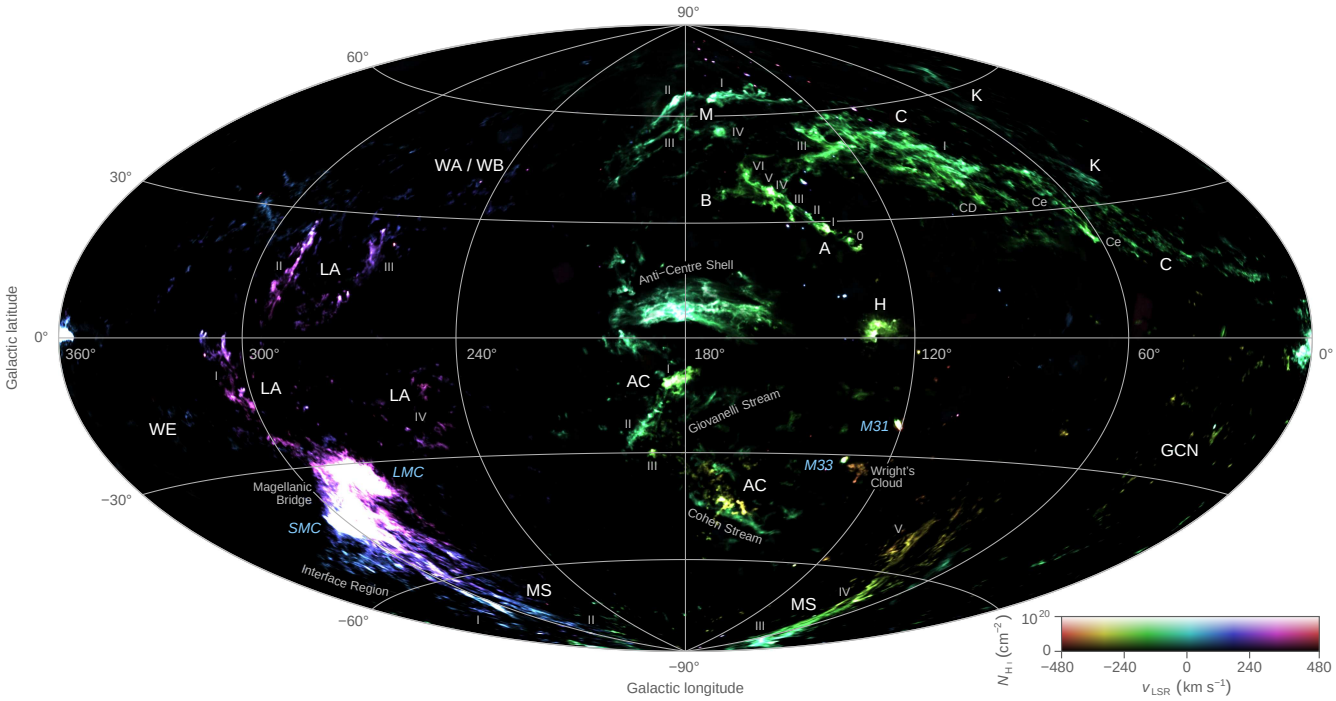

Figure 2. All-sky false-colour map of high-velocity gas presented in Hammer–Aitoff projection in Galactic coordinates centred on the Galactic anti-centre. Brightness and hue in the image represent H I column density (linear from 0 to 10^{20} cm^{-2}) and LSR radial velocity of the emission, respectively. Several major HVC complexes as well as a few notable individual structures and external galaxies are labelled.

3.3 Generation of HVC maps

After determination of the optimal set of parameters for the Galactic disc model, a custom script written in C++ was used to process the original HI4PI data with the aim of generating an all-sky map of HVCs. The script first reads an HI4PI sub-cube of $20° \times 20°$ into memory. It then loops across all spatial pixels of the cube, extracts the Galactic coordinates at each pixel, and applies Eq. 3 to determine the velocity range of Galactic emission at that position by moving outwards from the Sun along the line of sight in steps of 100 pc. All spectral channels located within that Galactic velocity range, expanded by the deviation velocity of 70 km s^{-1}, are then masked before the processed cube is written back to disk for subsequent analysis.

In order to facilitate the creation of two-dimensional maps of the HVC sky from the masked data cubes, the masked cubes were first smoothed spatially by a Gaussian of 48 arcmin FWHM and spectrally by a boxcar filter 5 channels (approximately 7.5 km s^{-1}) wide. Only those pixels of the original cube that had $T_B > 50$ mK in the smoothed copy of the cube were used in the generation of any two-dimensional maps created from the data cube. This approach ensures that the faint outer parts of diffuse H I sources are included in the map, while compact artefacts such as noise and radio frequency interference (RFI) are largely excluded. Lastly, any two-dimensional HVC maps created from the masked data cubes were concatenated to form a single, all-sky map.

The resulting two-dimensional all-sky HVC map in Hammer–Aitoff projection is presented in Fig. 2 in Galactic coordinates centred on the Galactic anti-centre. In this colour map, which was created to facilitate visual inspection of the HVC emission, brightness represents H I column density, while hue reflects the LSR radial velocity of the emission. This allows HVCs of different velocities to be distinguished by their different hues in regions of spatially overlapping emission. The naming of HVC features in the map is in accordance with Wakker (2001), Putman et al. (2003), Wakker (2004), Brüns et al. (2005), Venzmer et al. (2012) and For et al. (2013).

To provide data products that are more suitable for a quantitative analysis, a two-dimensional map of the 0th spectral moment was created as well. The 0th moment map was converted to H I column density in units of cm^{-2}, using the standard conversion factor of 1.823×10^{18} cm^{-2}/(K km s^{-1}), under the assumption that the emission is optically thin and fills the 16.2 arcmin beam. A labelled all-sky view of the resulting column density map in Hammer–Aitoff projection in Galactic coordinates is presented in the upper panel of Fig. A1 in Appendix A.

In a similar fashion one could generate a radial velocity map of the HVC sky from the 1st spectral moment. However, a general issue with the 1st moment is that the resulting values may be highly susceptible to the influence of noise in cases where either the H I signal is faint or the applied mask is too large. In addition, the 1st moment may produce arbitrary values in cases where multiple sources of emission exist along the line of sight. In order to avoid these issues, a velocity map was created by fitting a single Gaussian function to the brightest line component in each spectrum using a custom script written in PYTHON. The script will first identify the location of the brightest emission in the spectrum, then determine the mean and standard deviation of the emission within a window of ±20 channels around that position, and finally use those initial estimates to fit a Gaussian function

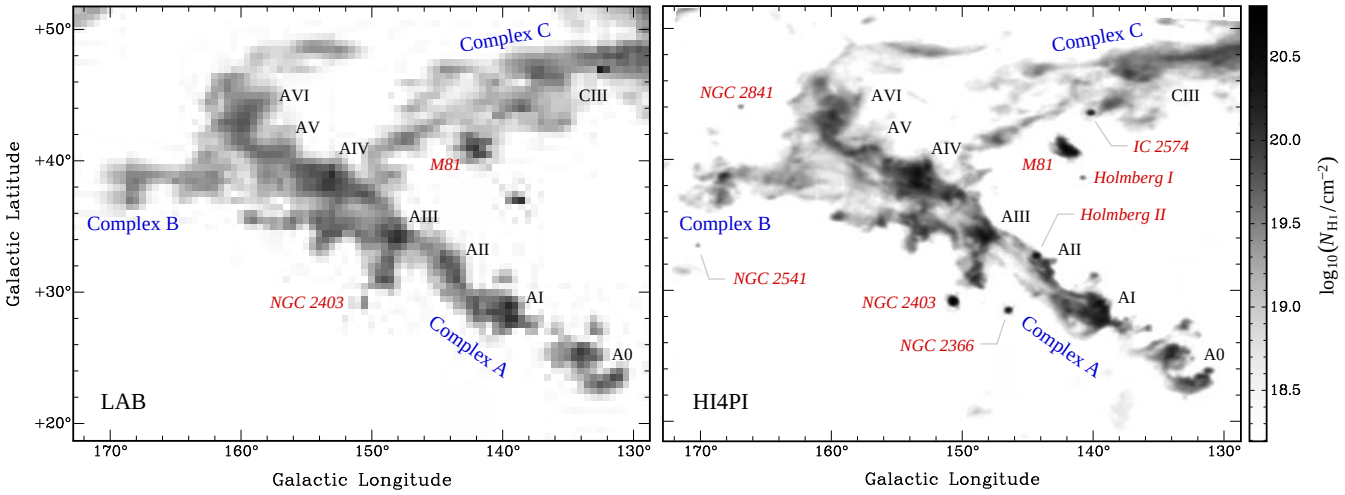

Figure 3. Comparison between the old HVC map from Westmeier (2007) based on LAB data (left) and the new map presented here based on HI4PI data (right) in the region of HVC complex A. The substantial improvement in angular resolution reveals a complex network of intricate gas filaments and clumps that are not resolved by the old LAB data. Note the large number of nearby galaxies visible in the high-resolution HI4PI data, the brightest of which have been labelled.

to the entire spectrum. Successful fits are accepted for spectra that have positive integrated flux, a peak brightness temperature exceeding three times the mean RMS of the HI4PI survey (i.e. $T_B \geq 130$ mK), and an initial estimate of the standard deviation of at least two channels (i.e. $\sigma \gtrsim 2.6$ km s^{-1}). The amplitude, mean and standard deviation from accepted Gaussian fits are then written into a FITS file for further analysis.

As the native LSR velocity frame of the HI4PI data is dominated by the projected rotation velocity of the Galactic disc, the resulting velocity map was converted to the more appropriate Galactic standard-of-rest (GSR) frame in units of km s^{-1}, assuming the standard orbital velocity of $v_\odot$ = 220 km s^{-1} in the direction of $(l, b) = (90°, 0°)$. The resulting GSR velocity map of the HVC sky in Galactic coordinates is presented in the bottom panel of Fig. A1 in Appendix A.

Finally, in order to facilitate studies of the Magellanic system, the H I column density and GSR velocity maps were converted from the native Galactic coordinate system, (l, b), to Magellanic coordinates, $(l_{\rm Mag}, b_{\rm Mag})$, as defined by Nidever et al. (2008). The resulting maps are presented in Fig. A2 in Appendix A. The Magellanic coordinate system is defined such that the Magellanic Stream and Leading Arm are approximately aligned with the equator at $b_{\rm Mag} \approx 0°$, while the Large Magellanic Cloud defines the origin of the longitudinal axis at $l_{\rm Mag} = 0°$. This avoids the usually strong distortions of parts of the Magellanic system in standard equatorial and Galactic coordinates and provides a more natural coordinate system suitable for studies of the Magellanic system. Note that the maps in Fig. A2 have been centred on $l_{\rm Mag} = 270°$ instead of 0° to prevent Complex C from being wrapped around the edge of the map.

4 RESULTS AND DISCUSSION

4.1 The HVC sky

The all-sky maps shown in Fig. 2 as well as Fig. A1 and A2 show the major HVC complexes in the sky in much greater detail than ever before. Dominant structures in the maps include the large HVC complexes A, C and M in the northern (celestial and Galactic) hemisphere, the anti-centre complex and shell near the Galactic anti-centre, and the Magellanic Clouds with the extended structures of the Magellanic Stream and Leading Arm mostly confined to the southern hemisphere. A few smaller or less sharply defined structures are visible as well, including HVC complexes H and K. Several HVC complexes with low deviation velocities, most of which kinematically overlap with Galactic disc emission, are largely missing from the map, including complexes L, WA, WB, WC, G, R, GCP as well as parts of complex H and the Giovanelli Stream.

The final maps are almost entirely free of residual emission from the Galactic disc. Notable contamination stems from peculiar-velocity gas near the Galactic centre, faint intermediate-velocity gas filaments near the north Galactic pole, and a few remnants of extra-planar gas associated with the Outer Arm near $(l, b) = (80°, 25°)$. Moreover, not all emission seen in the maps is due to high-velocity H I gas. On the one hand, low levels of RFI and residual stray radiation may still be present in some parts of the sky, in particular in the northern celestial hemisphere covered by EBHIS. On the other hand, several nearby galaxies at low radial velocities are included in the map as well, most prominently the Large and Small Magellanic Cloud as well as M31 and M33.

It should be noted that some of the HVC complexes partially extend into the velocity range of Galactic disc gas, which inevitably leads to the loss of some emission from the maps. As a consequence, the column density values in some regions of Fig. A1 and A2 may be lower limits while the velocities may be inaccurate. The Magellanic Stream in particular crosses from negative to positive LSR velocities near the south Galactic pole, inevitably resulting in flux loss. For the same reason, some neutral gas clouds located in the Galactic halo may be missing entirely, as their kinematics in combination with the viewing geometry may have placed them within the deviation velocity range applied here. This would effectively 'hide' those clouds within

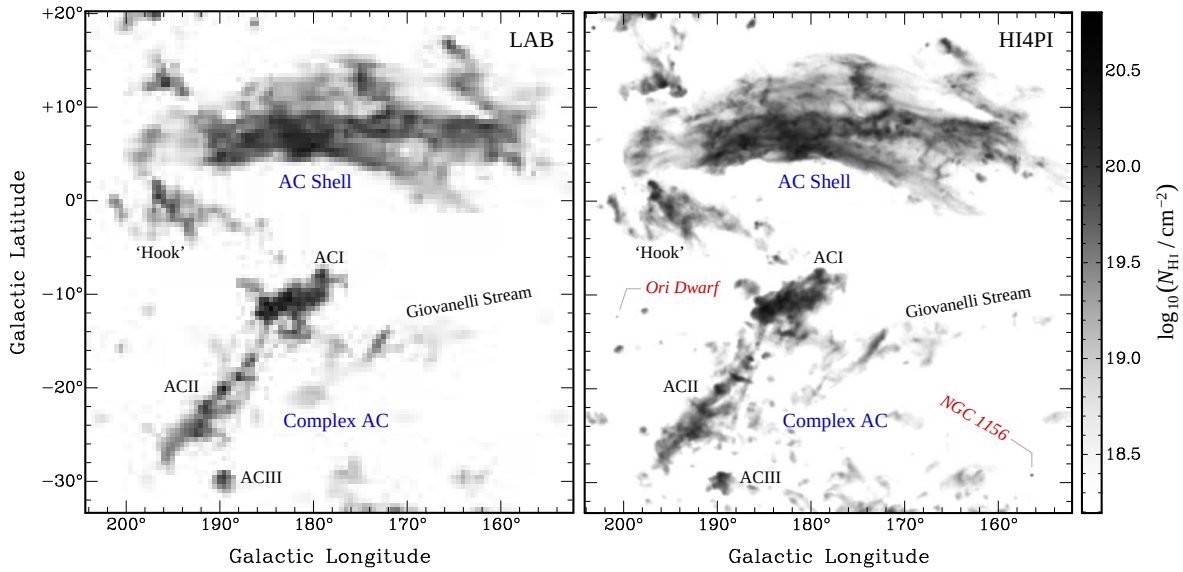

Figure 4. Same as in Fig. 3, but for a larger region around the northern section of the anti-centre (AC) complex and the adjacent anti-centre shell.

the velocity range of the Galactic disc, where they would no longer be discernible as high-velocity gas.

4.2 Comparison with LAB data

Using the regions around HVC complex A and the anti-centre (AC) complex as an example, Fig. 3 and 4 compare the quality of the previous all-sky map created by Westmeier (2007) based on LAB data with the new HI4PI-based map presented here. While the individual clouds of complex A were barely resolved by the 36 arcmin beam of the LAB survey, the new data resolve complex A into a remarkable network of intricate H I filaments and small clumps. Assuming a distance in the range of 4 to 10 kpc for complex A (van Woerden et al. 1999), the corresponding physical resolution would be in the range of about 20 to 50 pc. A similar effect can be seen in the anti-centre region, where the AC shell in particular breaks up into a system of fine, interwoven gas filaments that were too narrow to be resolved by the 36 arcmin beam of the LAB survey in the past.

An additional improvement in the quality of the map can be attributed to the full spatial sampling of the HI4PI survey data in contrast to the LAB data which were only sampled on a 30 arcmin grid. The undersampling of the LAB survey is clearly visible in the left-hand panels of Fig. 3 and 4. On top of the improvements in resolution and sampling, the HI4PI survey is also more sensitive than the LAB survey, resulting in a better column density sensitivity[2] of about 2.3×10^{18} cm^{-2} (as compared to about 3.7×10^{18} cm^{-2} for the LAB survey across a much larger beam solid angle). The significant improvement in both angular resolution and sensitivity is also highlighted by the large number of nearby galaxies visible in the HI4PI map in the right-hand panel of Fig. 3, only the brightest and most extended of which are also seen in the LAB data.

Lastly, the general agreement between the LAB and HI4PI maps is remarkable in view of the fact that a slightly different methodology was used by Westmeier (2007) for generating the LAB-based HVC map. Nevertheless, the same general features are visible in the two maps, indicating that most of the HVC structures in the sky are kinematically well-separated from the Galactic disc and thus appear in both maps.

4.3 Sky coverage fraction of HVCs

From the resulting HVC map one can immediately derive the sky coverage fraction of high-velocity H I emission as a function of column density. For this purpose, column density values were extracted from the map in *plate carrée* projection on a grid of Δb = 0.25 deg in Galactic latitude and $\Delta l\cos(b)$ = 0.25 deg in Galactic longitude, resulting in a total of about $4\pi/\Omega_{\rm grid} \approx 660{,}000$ largely independent data points across the full sky. The resulting sky coverage fraction, $f_{\rm sky}$, and cumulative sky coverage fraction, $\phi_{\rm sky}$, of HVC emission in excess of a given H I column density level are shown as the blue squares in Fig. 5. The cumulative sky coverage fraction for HVC emission of $N_{\rm H\,I} > 2\times10^{18}$ cm^{-2} is approximately 15 per cent. It decreases to about 7 per cent at $N_{\rm H\,I} > 10^{19}$ cm^{-2} and about 1 per cent at $N_{\rm H\,I} > 10^{20}$ cm^{-2}.

The original HVC map still contains some emission from sources other than HVCs, in particular nearby galaxies, residual emission from the Galactic disc and stray radiation residuals in the northern celestial hemisphere covered by EBHIS. Therefore, a cleaned HVC map was created by manually masking bright galaxies (including the LMC, SMC and Magellanic Bridge, but not the Interface Region, Magellanic Stream and Leading Arm), bright emission near the Galactic centre, residual emission from the Outer Arm and bright stray radiation residuals in the EBHIS data. The measurements of $f_{\rm sky}$ and $\phi_{\rm sky}$ resulting from the cleaned map

[2] H I column density sensitivities are specified for a signal of $5\times\sigma_{\rm RMS}$ across 20 km s^{-1} under the assumption that the emission is optically thin and fills the beam size.

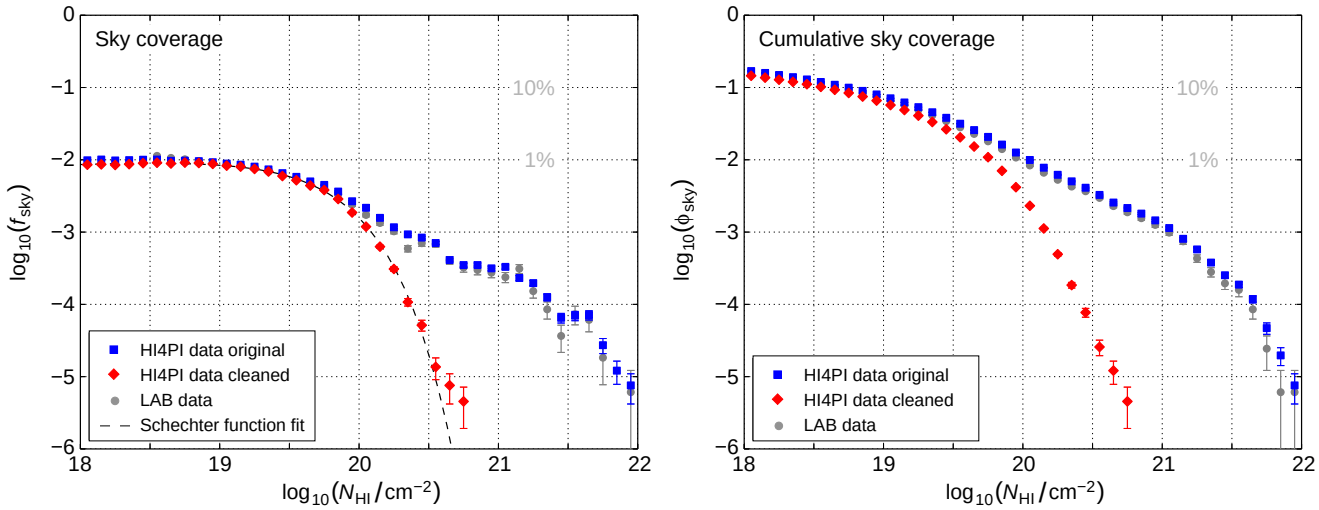

Figure 5. *Left:* Sky coverage fraction, $f_{\rm sky}$, of high-velocity gas as a function of H I column density in bins of $\Delta \log_{10}(N_{\rm H\,I}/{\rm cm}^{-2}) = 0.1$. *Right:* Cumulative sky coverage fraction, $\phi_{\rm sky}$, of high-velocity gas exceeding a given column density level. In both panels the blue squares represent the original data, while the red diamonds were derived from a data set with bright galaxies (including the Magellanic Clouds), stray radiation artefacts and residual Galactic emission from the Outer Arm and the Galactic centre region removed. The LAB-based HVC map from Westmeier (2007) is shown as the grey circles for comparison. Error bars are indicative of Poisson errors. The dashed, black line in the left-hand panel shows a Schechter function fitted to the red diamonds.

are shown as the red diamonds in Fig. 5. Most of the high-column density emission above 10^{20} cm^{-2} in the original map can be attributed to the Magellanic Clouds and Bridge, and there is no more emission above about 5×10^{20} cm^{-2} in the cleaned map. At the same time, removing known non-HVC emission from the map did not greatly change the column density distribution below about 3×10^{19} cm^{-2}. The resulting coverage fractions from the cleaned map are $\phi_{\rm sky} \approx 13$, 6 and 0.2 per cent for column densities of $N_{\rm H\,I} > 2 \times 10^{18}$, 10^{19} and 10^{20} cm^{-2}, respectively.

These results are comparable to the cumulative sky coverage of 15 per cent at $N_{\rm H\,I} > 2 \times 10^{18}$ cm^{-2} reported by Wakker (2004). Similar numbers were found by Wakker (1991) who derived either 18 or 11 per cent above $T_{\rm B} = 50$ mK (equivalent to about 2×10^{18} cm^{-2}) depending on whether the Magellanic Stream and Outer Arm were included or excluded from the analysis. A larger sky coverage fraction of 37 per cent above a significantly lower $5\,\sigma$ column density threshold of $7{\times}10^{17}$ cm^{-2} was found by Murphy et al. (1995) from pointed H I observations towards 102 quasars (also see Lockman et al. 2002).

For comparison, the analysis was repeated on the all-sky HVC map from Westmeier (2007) based on the LAB survey. The results are presented as the grey circles in Fig. 5 for the full map with the Magellanic Clouds included. The similarity between the HI4PI and LAB sky coverage factors is remarkable, confirming that both maps essentially trace the same structures on the sky. Upon closer inspection the LAB data points generally appear to be slightly below the HI4PI data points. The most likely explanation for this discrepancy is that the 36 arcmin beam size of the LAB survey is significantly larger than the 16.2 arcmin HI4PI beam, resulting in beam smearing effects and thus generally lower column density levels in the LAB survey for any emission that is not diffuse across the beam. Therefore, the LAB sky coverage curves in Fig. 5 are actually expected to be shifted slightly to the left in the direction of lower column densities.

Looking at the differential sky coverage fraction after removal of galaxies and artefacts again (red diamonds in the left-hand panel of Fig. 5), it would appear that the sky coverage of HVCs essentially follows a power law at lower column densities, with a distinct turnover point at just under 10^{20} cm^{-2}. We can therefore fit a Schechter function (Schechter 1976) of the form

$$f(n) = \ln(10) f^{\star} n^{\alpha+1} \exp(-n) \qquad (4)$$

to the data points in $\log_{10}(N_{\rm H\,I}/{\rm cm}^{-2})$ space to extract the basic parameters of this truncated power law. Here, $n = N_{\rm H\,I}/N^{\star}_{\rm H\,I}$ is the dimensionless H I column density, $N^{\star}_{\rm H\,I}$ denotes the location of the characteristic turnover point, α is the exponent of the power-law component of the function, and $f^{\star}$ is a global normalisation factor.

The fitted Schechter function is shown as the dashed, black line in the left-hand panel of Fig. 5 and yields a power-law exponent of $\alpha = -0.93$, a characteristic turnover point of $\log_{10}(N^{\star}_{\rm H\,I}/{\rm cm}^{-2}) = 19.7$ and a scaling factor of $f^{\star} = 5.0{\times}10^{-3}$ normalised per interval of $\Delta \log_{10}(N_{\rm H\,I}/{\rm cm}^{-2}) = 0.1$. Hence, at lower column densities, the differential sky coverage fraction is almost flat in logarithmic space (i.e., the power-law exponent is close to -1), with a turnover point at a characteristic column density level of $N^{\star}_{\rm H\,I} \approx 5 \times 10^{19}$ cm^{-2}. Consequently, there is no *preferred* column density of HVC emission. There is also no indication of another turnover near the sensitivity limit of the HI4PI data ($\approx 10^{18}$ cm^{-2}), which is consistent with the findings of Lockman et al. (2002) who, at a slightly lower median completeness limit of $8{\times}10^{17}$ cm^{-2}, report HVC emission in 37 per cent of their 860 quasar sightlines.

Table 1. List of FITS data products made available as supplementary material in the online version of this paper. The standard FITS projection codes used are `CAR` (*plate carrée*) and `AIT` (Hammer–Aitoff). File sizes are given for the compressed files in units of 1 MB = 2^{20} B.

Data product	Coordinate system	Proj.	Dimension (pixels)	File name	File size (MB)
$\log_{10}(N_{\rm H\,I}/{\rm cm}^{-2})$	Galactic	`CAR`	4323×2144	`hi4pi-hvc-nhi-gal-car.fits.gz`	7.7
$\log_{10}(N_{\rm H\,I}/{\rm cm}^{-2})$	Galactic	`AIT`	3891×1947	`hi4pi-hvc-nhi-gal-ait.fits.gz`	4.6
$\log_{10}(N_{\rm H\,I}/{\rm cm}^{-2})$	Magellanic	`CAR`	4323×2144	`hi4pi-hvc-nhi-mag-car.fits.gz`	7.9
$v_{\rm LSR}/({\rm km\,s}^{-1})$	Galactic	`CAR`	4323×2144	`hi4pi-hvc-vlsr-gal-car.fits.gz`	4.5
$v_{\rm LSR}/({\rm km\,s}^{-1})$	Galactic	`AIT`	3891×1947	`hi4pi-hvc-vlsr-gal-ait.fits.gz`	2.9
$v_{\rm GSR}/({\rm km\,s}^{-1})$	Galactic	`CAR`	4323×2144	`hi4pi-hvc-vgsr-gal-car.fits.gz`	4.6
$v_{\rm GSR}/({\rm km\,s}^{-1})$	Galactic	`AIT`	3891×1947	`hi4pi-hvc-vgsr-gal-ait.fits.gz`	3.0
$v_{\rm GSR}/({\rm km\,s}^{-1})$	Magellanic	`CAR`	4323×2144	`hi4pi-hvc-vgsr-mag-car.fits.gz`	4.7

5 DATA RELEASE

All-sky HVC maps are a useful tool for a wide range of scientific applications, including, among others, the study of the HVC population itself (Wakker 1991; Wakker & van Woerden 1991), comparison of the H I emission with optical and ultra-violet absorption lines of ionised gas in the Galactic halo (Fox et al. 2006; Lehner et al. 2012), cross-correlation of the H I emission with X-ray emission (Kerp et al. 1996, 1999; Shelton et al. 2012) and Hα emission (Tufte et al. 1998; Barger et al. 2012), and comparison of the H I gas with molecular gas (Wakker et al. 1997) and dust emission (Wakker & Boulanger 1986; Miville-Deschênes et al. 2005; Williams et al. 2012; Lenz et al. 2016) in the quest for evidence of star formation in HVC complexes such as the Magellanic Stream (Tanaka & Hamajima 1982; Brück & Hawkins 1983) and Leading Arm (Casetti-Dinescu et al. 2014).

In order to facilitate a wider scientific use of the new all-sky HVC maps by the community, H I column density maps and radial velocity maps in the LSR and GSR frames have been made publicly available in both *plate carrée* and Hammer–Aitoff projections (see Table 1 for details). The maps are provided as two-dimensional FITS images (*Flexible Image Transport System*; Wells et al. 1981) and are available as supplementary material in the online version of this paper. Column density and GSR velocity maps in *plate carrée* projection are also made available in Magellanic coordinates (using the definition of Nidever et al. 2008) in which the Magellanic Stream is aligned with the equator to facilitate studies of the Magellanic system. Note that for convenience the corresponding FITS files have Galactic coordinates defined in their header, as the FITS standard does not natively support the Magellanic coordinate system (Calabretta & Greisen 2002), while user-specific coordinate systems may not be supported by some of the third-party software commonly used to handle and display FITS images.

6 SUMMARY

In this paper a new all-sky map of Galactic HVCs based on the HI4PI survey is presented. For this purpose, a simple, cylindrical model of the Galactic disc with a disc radius of 20 kpc and a disc height of 5 kpc was created based on which the expected velocity range of Galactic emission was determined and masked after applying an additional deviation velocity of 70 km s^{-1}. All-sky H I column density and velocity maps of high-velocity gas were then generated from the masked cubes.

The resulting all-sky maps show the Milky Way's HVC population at an unprecedented angular resolution of 16.2 arcmin and a 5σ column density sensitivity of about 2.3×10^{18} cm^{-2}. Most of the HVC complexes are resolved into a network of H I filaments and clumps not seen in the previous HVC maps of Wakker (1991) and Westmeier (2007). The overall sky coverage fraction of high-velocity gas is approximately 15 per cent for emission of $N_{\rm H\,I} > 2\times10^{18}$ cm^{-2}, decreasing to about 13 per cent when the Magellanic Clouds and some additional non-HVC emission are excluded. The differential HVC sky coverage fraction as a function of column density essentially follows a truncated power law with an exponent of -0.93 and a characteristic turnover point at a column density level of about 5×10^{19} cm^{-2}.

FITS files of H I column density and velocity maps of the HVC sky in different coordinate systems and projections have been made publicly available to facilitate the scientific use of the new HVC map by the entire community. Users are requested to include a reference to this paper in any publication making use of these data files.

ACKNOWLEDGEMENTS

The author would like to thank L. Staveley-Smith for valuable discussions and comments on the manuscript. This work is based on publicly released data from the HI4PI survey which combines the Effelsberg–Bonn H I Survey (EBHIS) in the northern hemisphere with the Galactic All-Sky Survey (GASS) in the southern hemisphere. This publication is based on observations with the 100-m telescope of the MPIfR (Max-Planck-Institut für Radioastronomie) at Effelsberg. The Parkes Radio Telescope is part of the Australia Telescope which is funded by the Commonwealth of Australia for operation as a National Facility managed by CSIRO. This research has made use of the VizieR catalogue access tool, CDS, Strasbourg, France. The original description of the VizieR service was published in A&AS 143, 23. This research has made use of NASA's Astrophysics Data System Bibliographic Services. This research has made use of the NASA/IPAC Extragalactic Database (NED), which is operated by the Jet Propulsion Laboratory, California Institute of Technology, under contract with the National Aeronautics and Space Administration.

REFERENCES

Adams E. A. K., Giovanelli R., Haynes M. P., 2013, ApJ, 768, 77
Arnal E. M., Bajaja E., Larrarte J. J., Morras R., Pöppel W. G. L., 2000, A&AS, 142, 35
Bajaja E., Cappa de Nicolau C. E., Cersosimo J. C., Martin M. C., Loiseau N., Morras R., Olano C. A., Pöppel W. G. L., 1985, ApJS, 58, 143
Barger K. A., Haffner L. M., Wakker B. P., Hill A. S., Madsen G. J., Duncan A. K., 2012, ApJ, 761, 145
Barnes D. G., et al., 2001, MNRAS, 322, 486
Blitz L., Spergel D. N., Teuben P. J., Hartmann D., Burton W. B., 1999, ApJ, 514, 818
Braun R., Burton W. B., 1999, A&A, 341, 437
Bregman J. N., 1980, ApJ, 236, 577
Brück M. T., Hawkins M. R. S., 1983, A&A, 124, 216
Brüns C., et al., 2005, A&A, 432, 45
Calabretta M. R., Greisen E. W., 2002, A&A, 395, 1077
Casetti-Dinescu D. I., Moni Bidin C., Girard T. M., Méndez R. A., Vieira K., Korchagin V. I., van Altena W. F., 2014, ApJ, 784, L37
Clemens D. P., 1985, ApJ, 295, 422
Cox D. P., 1972, ApJ, 178, 159
Danly L., Albert C. E., Kuntz K. D., 1993, ApJ, 416, L29
For B.-Q., Staveley-Smith L., McClure-Griffiths N. M., 2013, ApJ, 764, 74
Fox A. J., Savage B. D., Wakker B. P., 2006, ApJS, 165, 229
Fox A. J., et al., 2016, ApJ, 816, L11
Fraternali F., Marasco A., Armillotta L., Marinacci F., 2015, MNRAS, 447, L70
HI4PI Collaboration 2016, A&A, 594, A116
Hartmann D., Burton W. B., 1997, Atlas of Galactic Neutral Hydrogen. Cambridge University Press
Hulsbosch A. N. M., 1968, Bull. Astron. Inst. Netherlands, 20, 33
Hulsbosch A. N. M., Wakker B. P., 1988, A&AS, 75, 191
Kalberla P. M. W., Haud U., 2015, A&A, 578, A78
Kalberla P. M. W., Burton W. B., Hartmann D., Arnal E. M., Bajaja E., Morras R., Pöppel W. G. L., 2005, A&A, 440, 775
Kalberla P. M. W., et al., 2010, A&A, 521, A17
Kerp J., Mack K.-H., Egger R., Pietz J., Zimmer F., Mebold U., Burton W. B., Hartmann D., 1996, A&A, 312, 67
Kerp J., Burton W. B., Egger R., Freyberg M. J., Hartmann D., Kalberla P. M. W., Mebold U., Pietz J., 1999, A&A, 342, 213
Kerp J., Winkel B., Ben Bekhti N., Flöer L., Kalberla P. M. W., 2011, Astron. Nachr., 332, 637
Kerr F. J., Lynden-Bell D., 1986, MNRAS, 221, 1023
Lehner N., Howk J. C., 2010, ApJ, 709, L138
Lehner N., Howk J. C., Thom C., Fox A. J., Tumlinson J., Tripp T. M., Meiring J. D., 2012, MNRAS, 424, 2896
Lenz D., Flöer L., Kerp J., 2016, A&A, 586, A121
Lockman F. J., Murphy E. M., Petty-Powell S., Urick V. J., 2002, ApJS, 140, 331
Marasco A., Fraternali F., 2017, MNRAS, 464, L100
Mathewson D. S., Cleary M. N., Murray J. D., 1974, ApJ, 190, 291
McClure-Griffiths N. M., et al., 2009, ApJS, 181, 398
Miville-Deschênes M.-A., Boulanger F., Reach W. T., Noriega-Crespo A., 2005, ApJ, 631, L57
Morras R., Bajaja E., Arnal E. M., Pöppel W. G. L., 2000, A&AS, 142, 25
Muller C. A., Oort J. H., Raimond E., 1963, C. R. Acad. Sci., 257, 1661
Murphy E. M., Lockman F. J., Savage B. D., 1995, ApJ, 447, 642
Nidever D. L., Majewski S. R., Burton W. B., 2008, ApJ, 679, 432
Oort J. H., 1966, Bull. Astron. Inst. Netherlands, 18, 421
Peek J. E. G., Bordoloi R., Sana H., Roman-Duval J., Tumlinson J., Zheng Y., 2016, ApJ, 828, L20
Putman M. E., et al., 2002, AJ, 123, 873
Putman M. E., Staveley-Smith L., Freeman K. C., Gibson B. K., Barnes D. G., 2003, ApJ, 586, 170
Savage B. D., de Boer K. S., 1981, ApJ, 243, 460
Schechter P., 1976, ApJ, 203, 297
Sembach K. R., et al., 2003, ApJS, 146, 165
Shelton R. L., Kwak K., Henley D. B., 2012, ApJ, 751, 120
Tanaka K. I., Hamajima K., 1982, PASJ, 34, 417
Thom C., Peek J. E. G., Putman M. E., Heiles C., Peek K. M. G., Wilhelm R., 2008, ApJ, 684, 364
Tufte S. L., Reynolds R. J., Haffner L. M., 1998, ApJ, 504, 773
Venzmer M. S., Kerp J., Kalberla P. M. W., 2012, A&A, 547, A12
Wakker B. P., 1991, A&A, 250, 499
Wakker B. P., 2001, ApJS, 136, 463
Wakker B. P., 2004, HVC/IVC Maps and HVC Distribution Functions. Kluwer Academic Publishers, pp 25–54
Wakker B. P., Boulanger F., 1986, A&A, 170, 84
Wakker B. P., van Woerden H., 1991, A&A, 250, 509
Wakker B. P., van Woerden H., 1997, ARA&A, 35, 217
Wakker B., Howk C., Schwarz U., van Woerden H., Beers T., Wilhelm R., Kalberla P., Danly L., 1996, ApJ, 473, 834
Wakker B. P., Murphy E. M., van Woerden H., Dame T. M., 1997, ApJ, 488, 216
Wakker B. P., et al., 2007, ApJ, 670, L113
Wakker B. P., York D. G., Wilhelm R., Barentine J. C., Richter P., Beers T. C., Ivezić Ž., Howk J. C., 2008, ApJ, 672, 298
Wells D. C., Greisen E. W., Harten R. H., 1981, A&AS, 44, 363
Westmeier T., 2007, PhD thesis, Rheinische Friedrich-Wilhelms-Universität Bonn
Williams R. J., Mathur S., Poindexter S., Elvis M., Nicastro F., 2012, AJ, 143, 82
Winkel B., Kerp J., Flöer L., Kalberla P. M. W., Ben Bekhti N., Keller R., Lenz D., 2016, A&A, 585, A41
de Boer K. S., 2004, A&A, 419, 527
de Heij V., Braun R., Burton W. B., 2002a, A&A, 391, 159
de Heij V., Braun R., Burton W. B., 2002b, A&A, 392, 417
van Woerden H., Schwarz U. J., Peletier R. F., Wakker B. P., Kalberla P. M. W., 1999, Nature, 400, 138
van Woerden H., Wakker B. P., Schwarz U. J., de Boer K. S., eds, 2004, High Velocity Clouds. Astrophysics and Space Science Library Vol. 312, Kluver Academic Publishers

SUPPORTING INFORMATION

Additional Supporting Information may be found in the online version of this paper:

As detailed in Section 5, FITS images of the new all-sky map of HVCs presented in this paper are made available as supplementary material in the online version of this paper. An overview of the individual data products and corresponding FITS files is provided in Table 1.

Please note: Oxford University Press are not responsible for the content or functionality of any supporting materials supplied by the authors. Any queries (other than missing material) should be directed to the corresponding author for the paper.

APPENDIX A: COLUMN DENSITY AND VELOCITY MAPS

H I column density and GSR radial velocity maps of the high-velocity sky in Hammer–Aitoff projection in both Galactic and Magellanic coordinates are presented in this appendix.

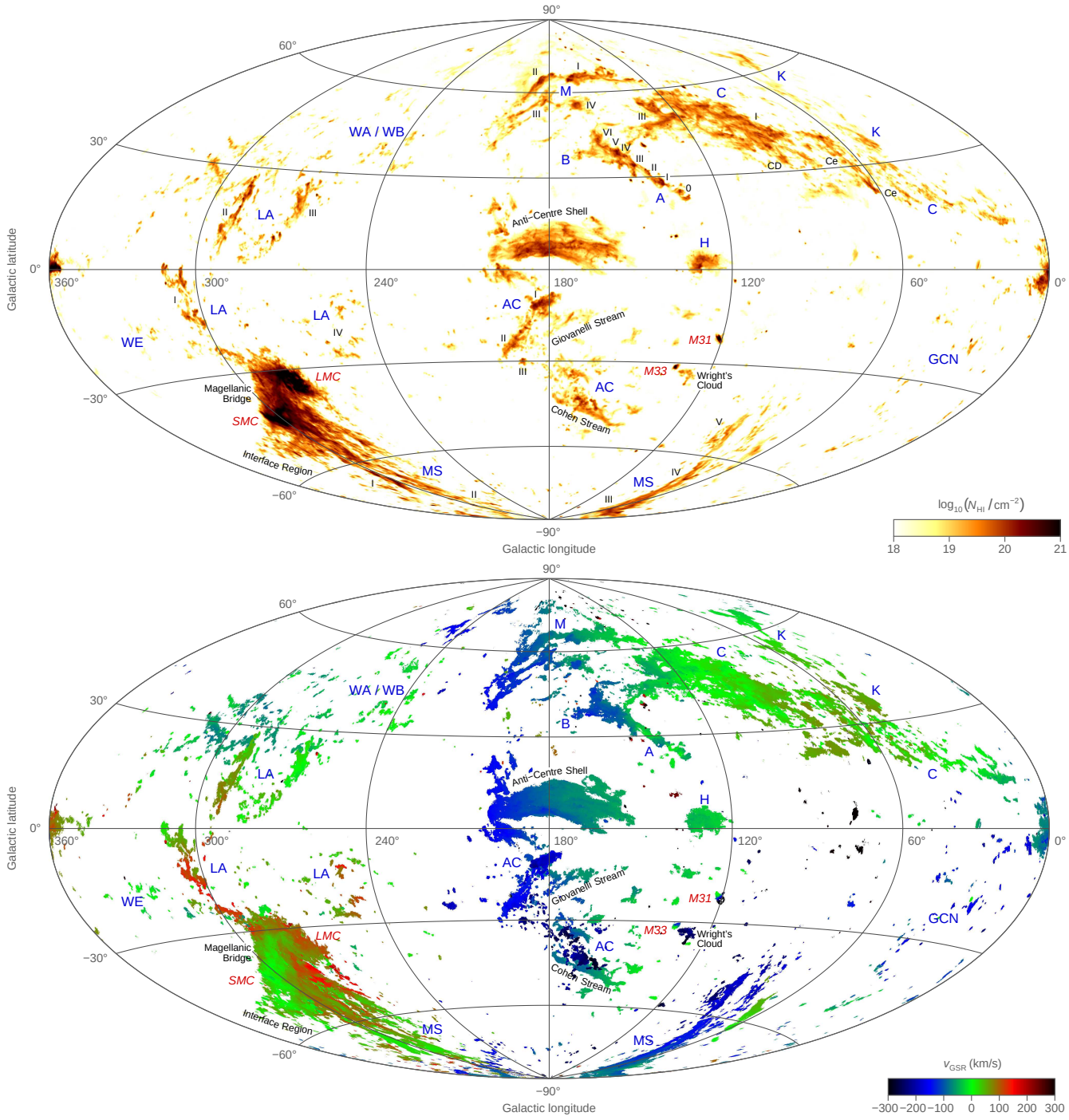

Figure A1. All-sky maps of high-velocity gas presented in Hammer–Aitoff projection in Galactic coordinates centred on the Galactic anti-centre. Top: H I column density, derived from the 0$^{\rm th}$ spectral moment, in the range of $\log_{10}(N_{\rm H\,I}/{\rm cm}^{-2})$ = 18 to 21 under the assumption that the emission is optically thin and fills the 16.2-arcmin beam. Bottom: Radial velocity in the GSR frame, derived from Gaussian fits, in the range of $v_{\rm GSR}$ = −300 to +300 km s^{-1}. Several major HVC complexes as well as a few notable individual structures and external galaxies are labelled. Note that a few remaining artefacts caused by RFI and residual stray radiation were manually removed from both maps for presentation purposes, but they are still present in the released FITS images.

This paper has been typeset from a TEX/LATEX file prepared by the author.

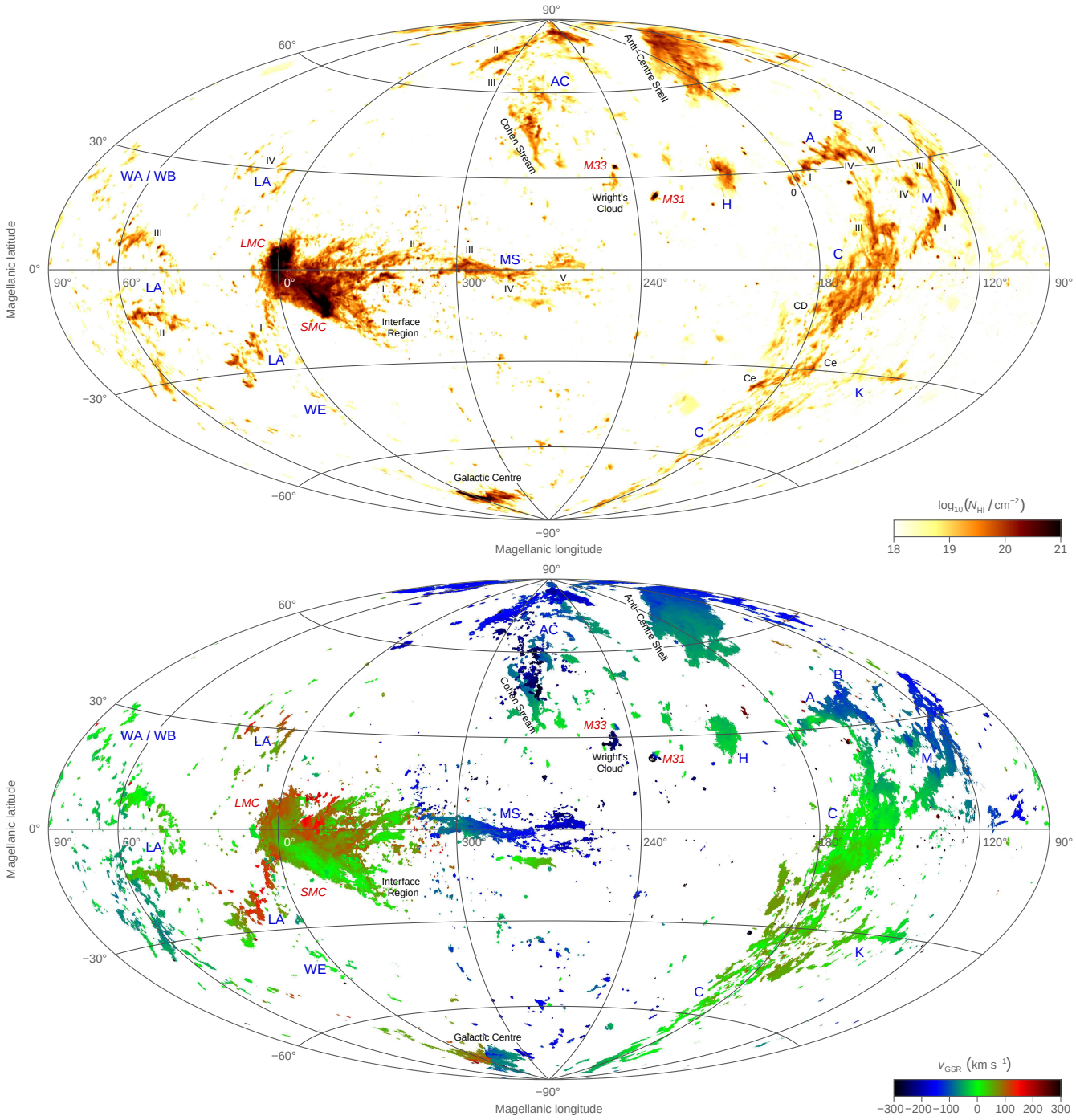

Figure A2. Same as in Fig. A1, but using the Magellanic coordinate system as defined by Nidever et al. (2008). The coordinate system is chosen such that the Magellanic Stream is aligned with the equator to facilitate studies of the Magellanic system. Note that the map is centred on 270° in Magellanic longitude, as otherwise complex C would be wrapped around the edge of the map.